Amino acid appended perylene bisimides: self-assembly, immobilization on nanocrystalline TiO2, and electrochromic properties

Ross Lundy,[a] Emily R. Draper* [b] and James J. Walsh* [c, d]

a. AMBER & CRANN, School of Chemistry, Trinity College Dublin, Dublin 2, Ireland.

b. School of Chemistry, University of Glasgow, Glasgow, UK.

c. National Centre for Sensor Research, Dublin City University, Glasnevin, Dublin 9, Ireland.

d. School of Chemical Sciences, Dublin City University, Glasnevin, Dublin 9, Ireland.

Abstract

Titanium dioxide (TiO_2) nanoparticle films have been used as a conducting support for the immobilisation of alanine-appended perylene bisimides (PBI-A) via dip-coating and carboxylate chemisorption. The solvent- and concentration-dependent supramolecular structures of aggregated PBI-A were successfully translated onto the TiO_2 electrodes, providing a method to control PBI-A assembly on a surface suitable for multiple functionalities. Electron microscopy revealed the extent of aggregation on the surface, and how this affects electrochemical properties. The films showed electrochemical reversibility by cyclic voltammetry, and preliminary electrochromic studies show that three colour states could be accessed. Strategies to improve the overall device performance are discussed.

Introduction

Perylene bisimides (PBIs) consist of a perylene core functionalised with two imide groups, onto which an extremely wide range of functionalities can be appended.[1] The addition of various groups to the imides can be used to tune the solubility of the species and we have shown previously that the addition of amino acid groups can render amino acid appended PBIs highly soluble in water.[2] This makes them considerably simpler to process than conventional perylenes, which suffer from extremely low solubility in most common solvents, while retaining many of the desirable optical and electronic properties of the perylene (high molar absorption coefficients, intense fluorescence, multiple redox states, propensity to assemble into complex structures, etc).[1] The combination of ease of functionalisation with the retention of the outstanding optical properties of the perylene core have led to a huge increase in interest in the use of PBIs spanning many fields of chemistry which exploit optical and/or electrical characteristics,[3] and PBIs have been reported for use in organic photovoltaics,[4] sensing,[5] luminescent materials,[6] n-type photoconductivity,[7, 8] microwave conductivity,[9] dye-sensitised solar cells (DSSCs),[10] photocatalysis[2] and photoelectrochemistry (PEC).[11]

PBIs are well-known to self-assemble, primarily through π-π interactions. These aggregates can range from molecular dimers to superstructures on the micron length scale.[1] The types and degree of assembly are influenced by a wide range of factors including solvent dielectric, pH, concentration, type of PBI functionalization, solution temperature, etc. By adjusting these parameters, therefore, control can be exercised over the type of assembled aggregates formed. This is of critical importance for the integration of PBIs into functional devices as different aggregated PBI states exhibit

considerably different chemical properties such as luminescence quantum yields, absorption maxima, and redox potentials. Additionally, very large superstructures will affect long-range phenomena such as electron hopping through films, diffusion, surface area for catalytic reactions, etc. There are many literature examples of controlling PBI stacking through synthetic modification of the perylene bay positions with various functionalities, but this can be synthetically challenging.[12] An attractive proposition is to control the aggregation of simple PBIs through adjustments to solution concentration, solvent or pH. This has been shown previously for a range of PBIs;[7] however, the translation of the PBI supramolecular characteristics from solution onto a surface remains highly challenging, as aggregation properties tend to change upon drying of PBI solutions.

Nanocrystalline semiconductor electrodes are an excellent substrate for the immobilisation of molecular species from solution by simple dip-coating. By far the most commonly used semiconductor for immobilisation is TiO_2, especially in the field of DSSCs.[13] TiO_2 is also increasingly being recognised as an excellent substrate for use with materials exhibiting redox potentials negative of, or close to, the conduction band edge; this has led to the use of TiO_2 as an electrode support for CO_2 reduction electrocatalysis[14, 15] and electrochromic molecular materials.[16] Adsorption onto nanoparticulate oxide films, such as TiO_2, is typically achieved through dip-coating and chemisorption to the surface via carboxylate or phosphonate linkages. PBIs have been immobilised onto various metal oxides (In:SnO_2, WO_3, Al_2O_3, NiO, TiO_2) for use in fundamental photophysical studies and dye-sensitised PEC cells, typically using phosphonate linkers.[11, 17, 18, 19] There is also at least one example of PBI-based n-type electrochromics, through polymerisation of thin (38 nm) PBI films onto In:SnO_2.[20] In this study, we utilise nanoparticulate TiO_2 substrates to immobilise various aggregated forms of PBI-A (Fig. 1(b)). We show that the structure of aggregated PBI-A on the surface can be controlled using equimolar solutions of different solvents and various soaking times and, importantly, that the degree of surface aggregation is translated from solution onto the TiO_2 surface. Finally, the films can be used to access three different electrochromic colour states – two PBI-based and one TiO_2-based.

Results and discussion

Perylenes and other planar organic species are well known to self-assemble into π-stacked structures when dissolved in solution.[21] We have previously used a combination of UV/Vis and fluorescence spectroscopies to help characterise the type and degree of PBI-A aggregation when dissolved in aqueous solution as a function of concentration.[8] PBI-A tends to form H-aggregates at most concentrations studied,[1] consisting of slip-stacked helical bundles, with monomer-like spectroscopy not observed until H_2O solutions were diluted to 10^{-7} M (Huang-Rhys factor in 10^{-7} M/H_2O was 1.25). On the order of 10^{-4} M, the concentrations used for soaking in this contribution, the PBI-A is stacked into oligomeric aggregates, as suggested by the Huang-Rhys factor of the S_1 transition of 0.71 (Fig. 1 (a), Table S1). The highly-aggregated nature of 10^{-4} M PBI-A in H_2O translates onto the TiO_2 (ESI) surface, with deep pink coloured TiO_2/PBI-A electrodes exhibiting absorption spectra consistent with highly aggregated PBI-A adsorbed on the surface (Huang-Rhys factor = 0.82 on TiO_2, Fig. 1 (b) & Table S1, herein labelled soaked films of type A). ATR-FTIR spectroscopy of a soaked film revealed the presence of surface-bound PBI-A, and the absence of the symmetric C=O stretching mode suggests adsorption PBI-A to TiO_2 via a monodentate carboxylate linkage (full FTIR discussion, ESI).

In direct contrast, 10^{-4} M methanol solutions of PBI-A appear yellow-orange to the naked eye (Fig. 1 (a)) due to an extremely intense fluorescence (vide infra) which obscures the pink colour of the solution. UV/Vis spectroscopy of the 10^{-4} M PBI/MeOH solution revealed well-resolved fine structure with sharper, more intense bands than the equivalent H_2O solution, consistent with a monomer-like configuration (Huang-Rhys factor = 1.41, Table S1). Soaking a TiO_2 electrode soaking at 10, 20 and 30 minutes revealed monomer-like PBI-A adsorbed on the surface (Huang-Rhys factors = 1.41, 1.43, 1.31),

while 12 hr soaking in this solution yielded an electrode with very high absorption and an increased, but still relatively minor, degree of aggregation (Huang-Rhys factor = 1.01) reminiscent of dimeric PBI aggregates observed previously.[12] These results indicate that through control of soaking time and solvent, different aggregated states of PBI-A can be translated onto the electroactive surface, and that comparable overall molar absorptivities can be obtained for different PBI-A aggregated structures on TiO_2 (Fig. 1 (b)). In contrast to the 10^{-4} M MeOH solution, PBI-A/TiO_2 films soaked from 10^{-4} M MeOH (herein soaked films of type B) did not appear fluorescent due to the ability of PBI-A to inject photogenerated electrons into the TiO_2 conduction band (PBIs have been used successfully in DSSCs previously).[10] ATR-FTIR spectroscopy of the type B soaked PBI-A/TiO_2 was practically indistinguishable from the type A soaked sample, indicating the same monodentate carboxylate binding dominates. Fluorescence spectroscopy of the soaking solutions at 10^{-4} M (Fig. S2) revealed significant differences in absolute intensity, as anticipated based on the contrasting appearances of the solutions. The emission spectra showed fine structure with maxima at 547, 584 nm (H_2O), or 538, 571 nm (MeOH). At these concentrations, there was no evidence for excimer fluorescence at longer wavelengths.[8] Fluorimetry could not be obtained of PBI-A/TiO_2 due to electron injection; therefore PBI-A was soaked onto solid SiO_2 films (Fig. S3), which revealed similar emission maxima for each solvent (H_2O = 532, 568 nm; MeOH = 535, 572 nm).

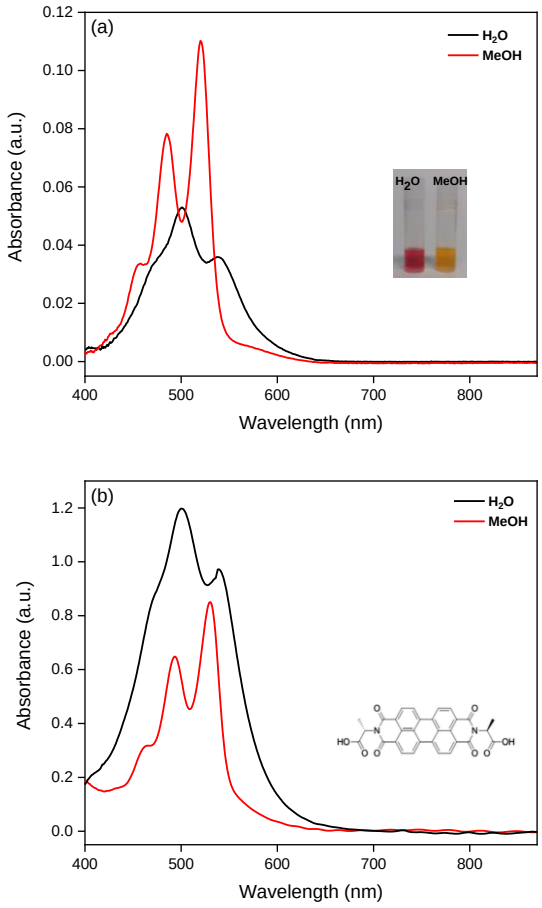

Fig. 1 (a): UV/Vis spectroscopy of soaking solutions showing differences in molar absorptivity and in the degree of aggregation as a function of solvent. Inset: Equimolar (10^{-4} M) soaking solutions of PBI-A. (b): Spectra of films soaked for 30 mins (MeOH) or 12 hours (H_2O) show that the aggregation of the PBI-A in solution is transferred to the surface (spectra recorded in air). Inset: Structure of PBI-A.

Initially, a type A TiO_2 film was studied using CV in 0.1 M KCl/H_2O as the supporting electrolyte. While the CV revealed the two redox processes known for amino acid-appended PBIs,[2] the film was unstable towards redox cycling in aqueous electrolyte, and desorption was observed visually after just two cycles (Fig. S4). CV of an equivalent film using 0.1 M TBA PF_6/MeCN electrolyte revealed a considerably different electrochemical response. The redox peaks associated with PBI-A could only be observed at very slow scan rates and were separated by hundreds of mV, indicating very high resistance in the films. This may be due to stacked PBI aggregates present on the surface which could potentially block the TiO_2 mesopores, restricting electrolyte diffusion through the film. By changing to 0.1 M $LiClO_4$/MeCN as supporting electrolyte the CV response was considerably improved while also avoiding the desorption of the film observed in aqueous electrolyte (Fig. S4). This improved response is likely due to facile permeation of the smaller ionic radii electrolyte ions through the film, as is typically observed for systems using mesoporous TiO_2 electrodes.[22] CVs of a type A TiO_2 electrode in 0.1 M $LiClO_4$/MeCN as supporting electrolyte showed that the resistance of the film was still high, with a peak-to-peak separation of ca. 350 mV at 50 mV.s^{-1}, which dropped to ca. 70 mV at 5 mV.s^{-1} (Fig. 2 (a)). PBI-A and related species are known to exhibit two sequential and reversible one-electron reductions which closely overlap and sometimes are not resolved, corresponding to the stepwise formation of the PBI radical anion ($PBI^{\cdot-}$) and dianion (PBI^{2-}), respectively.[2] Using a type A TiO_2 electrode, we could observe both reductions separated by ca. 50 mV when aqueous 0.1 M KCl was used as electrolyte. However, using 0.1 M $LiClO_4$/MeCN as electrolyte the reductions were overlapped except at very slow (5 mV.s^{-1}) scan rates. In all cases, the re-oxidation peaks are too closely overlapped to be resolved. Scan rate dependent CVs in 0.1 M $LiClO_4$/MeCN showed a linear relationship between scan rate and peak current, in-line with a surface-confined electrochemical response according to Eqn. 1,[16] which can also be used to estimate the geometric surface coverage, Γ, of electroactive PBI:

$$\boldsymbol{i = \left(\frac{n^2F^2}{4RT}\right)vA\Gamma} \qquad (1)$$

Where n is the number of electrons transferred, F is Faraday's constant (96485 C.mol^{-1}), R is the universal gas constant (8.314 J.mol^{-1}.K^{-1}), T is the temperature in Kelvin, and A is the geometric surface area in cm^2. Using Eqn. 1 yields PBI Γ values of ca. 3.5 x 10^{-9} mol.cm^{-2}, which is similar to recent examples of PBIs adsorbed on TiO_2 for photoelectrochemical applications.[19]

CVs using a monomer-like film – a type B electrode soaked for 30 mins and shown to be largely non-aggregated using UV/Vis spectroscopy - revealed broadly similar behaviour (Fig. 2 (b)). The currents passed suggest similar quantities of electroactive material are adsorbed on the surface. The resistance was still high in this case; however, $E_{OX\text{-}RED}$ decreased relative to the highly aggregated sample soaked from H_2O, suggesting that the electrochemical reversibility of the MeOH soaked film is superior to that of the H_2O soaked film (i.e.: decreased film resistance). For the MeOH soaked electrode, Γ values of ca. 2.7 x 10^{-9} mol.cm^{-2} using Eqn. 1. For comparison, PBI-A Γ can also be estimated using Eqn. 2:

$$\boldsymbol{\Gamma = \frac{Q}{nFA}} \qquad (2)$$

Using Eqn. 2 and slow scan rate (5 mV.s^{-1}) CV data, the values obtained were as follows: H_2O Γ = 5.3 x 10^{-9} mol.cm^{-2}; MeOH Γ = 6.8 x 10^{-9} mol.cm^{-2}. These agree with the scan rate data from Eqn. 1 within a factor of two and are within an order of magnitude of adsorption loadings of PBIs on TiO_2 reported

previously.[19] This is important as estimation of Γ using UV/Vis is severely restricted due to ε changing with concentration.

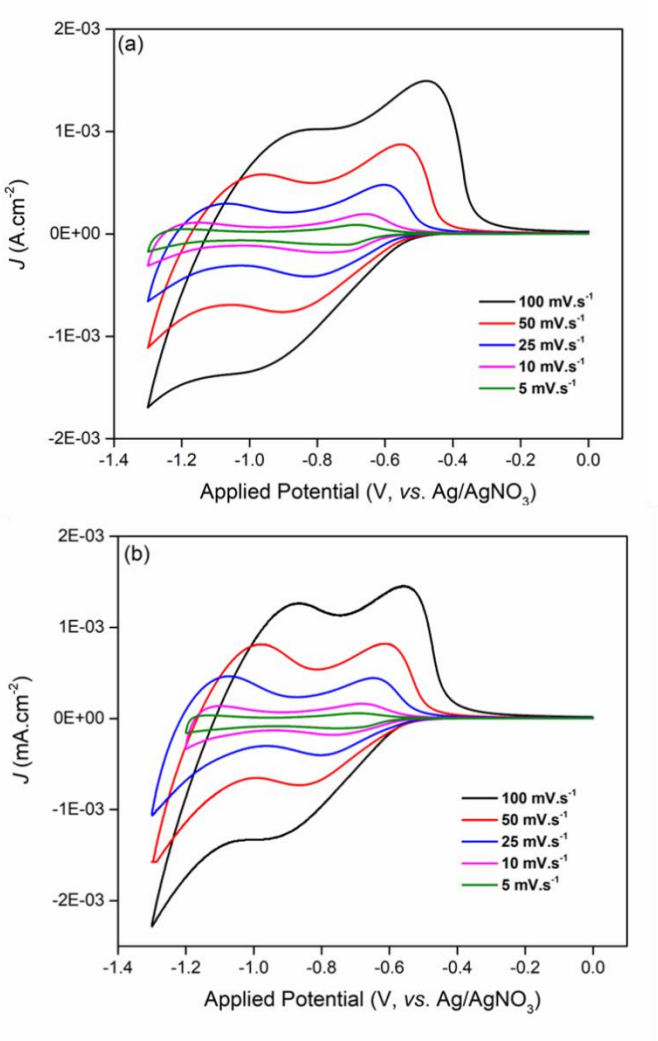

Fig. 2: CVs of (a) type A and (b) type B PBI-A/TiO_2 at 100, 50, 25, 10 and 5 $mV.s^{-1}$. Supporting electrolyte was 0.1 M $LiClO_4$/MeCN (Ar-purged), CE = Pt, RE = $Ag/AgNO_3$. Minor differences in geometric surface area have been normalised to current density (J).

Field-emission scanning electron microscopy (FESEM) of the films was used to investigate the effects of soaking from highly aggregated (type A) or monomer-like (type B) solutions of PBI-A at the same concentrations (10^{-4} M). As shown using UV/Vis spectroscopy (Fig. 1), the highly aggregated nature of PBI in type A soaking solutions is directly transferred onto the TiO_2, and this is reflected in the FESEM images. The mesopores in a TiO_2 film are typically on the order of tens of nm in diameter and permit facile electrolyte diffusion through these thick films.[13] However, when coated with highly aggregated PBI-A from type A soaking solutions, these pores are largely blocked by the self-assembled PBI structures (Fig. 3 (a)), which we showed previously using neutron scattering measurements to consist of worm-like micelles with a Kuhn length parameter on the order of 10 nm long in solution, and on the order of several microns in length when solutions were dried.[7, 8] It is likely that the effects of these large aggregates in blocking the TiO_2 mesopores is what causes such high resistance to be observed in the electrochemical measurements, and this is corroborated by changing from bulky

tetraalkylammonium electrolyte ions to smaller radius Li^+ resulting in improved CV reversibility, which has been observed using unmodified TiO_2 previously.[23]

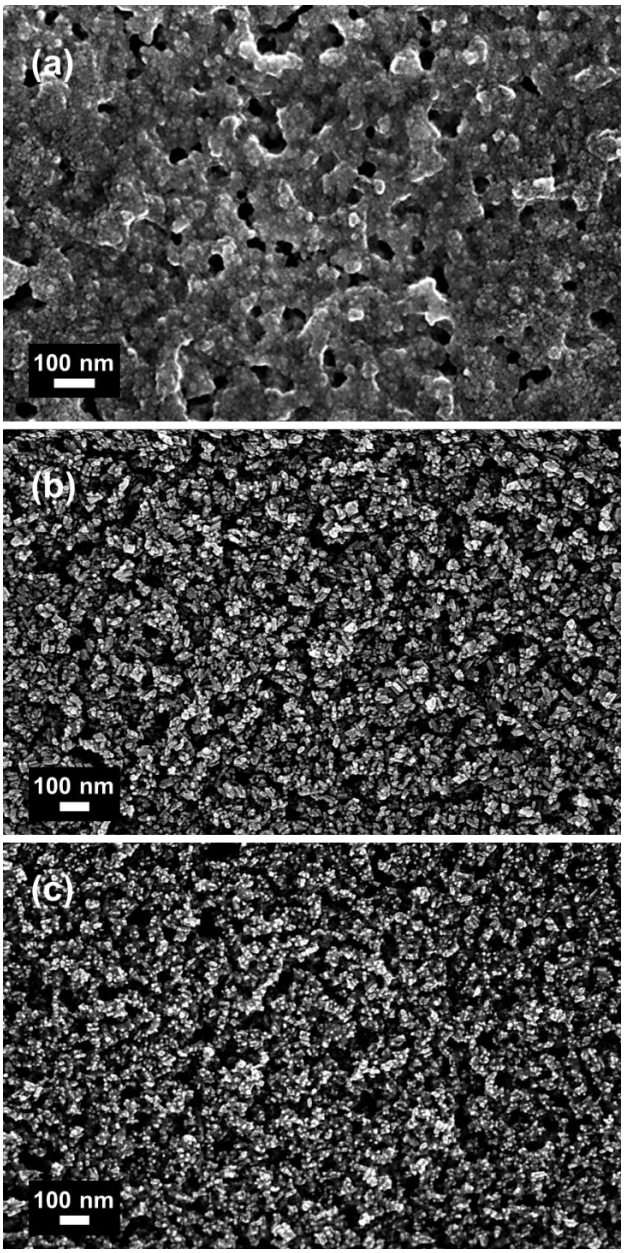

Fig. 3: FESEM of type A soaked PBI-A/TiO_2 (a), type B soaked PBI-A/TiO_2 (b) and unmodified TiO_2 (c).

In contrast, a TiO_2 film soaked from lower concentration 10^{-5} M/H_2O PBI solution (type C conditions) resulted in a lightly coloured electrode unsuitable for electrochromism (Fig. S5), and while the FESEM image of this electrode (Fig. S6) revealed that the mesopores remain partially blocked, the effect is less than as shown in Fig. 3. In comparison, FESEM of type B soaked TiO_2 revealed an unblocked mesoporous TiO_2 structure (Fig. 3 (b)), in line with our UV/Vis and CV studies using MeOH-soaked films. This film was largely indistinguishable from an unmodified TiO_2 electrode (Fig. 3 (c)) and suggests that monomer-like adsorbed PBI-A from MeOH soaking solutions should facilitate electron transfer processes and faster electrochemical responses.

Electrochromic (EC) devices, whereby the colour of a material can be modulated using an applied potential, have gained increased attention in recent years, especially with respect to smart windows, EC mirrors, digital displays, etc.[24, 25, 26] Amongst the most commonly used EC materials are oxides such as WO_3,[27] and recently a shift towards organic EC materials based mainly on oligothiophene polymers,[28] with materials covering the full palette of colours reported.[29, 30] Other materials commonly studied include viologens,[31] metallopolymers based on Ru(II) polypyridyl derivatives,[32] polyoxometalates,[16] Prussian blue,[33] and polyaniline.[34] These materials have the advantage of being fully soluble, hence they can be processed onto surfaces using conventional wet chemistry techniques, rendering them suitable for roll to roll spraying, or printing on flexible conducting substrates.

The electrochromic response of type A soaked TiO_2 films was measured in a spectroelectrochemical cell using N_2-purged 0.1 M $LiClO_4$/MeCN as the supporting electrolyte. Bulk electrolysis of a type A soaked film at 25 mV intervals revealed the grow-in of species known to correspond to $PBI^{\cdot-}$, PBI^{2-} and TiO_2 e^- (see Fig. 4), corresponding to colour changes from red-pink to purple to navy.[2, 7] The dark navy colour observed upon extensive reduction has been shown previously to be due to reduction of the TiO_2 (i.e.: the presence of e^- in the TiO_2 conduction band).[15] Fig. S7 (a) shows the stepwise reduction of the TiO_2 and the grow-in of this band, and a plot of absorbance at 900 nm vs. applied potential (Fig. S7 (b)) shows that the grow-in of the band mirrors the conduction band edge as measured by cyclic voltammetry, this feature is therefore unambiguously assigned to TiO_2 e^-. Electrochromic switching was performed at 715 nm for 500 cycles (Fig. S8). After 500 cycles, the type A soaked film appeared to lose its conductivity, as evidenced by the change in CV response from reversible to irreversible (Fig. S9). UV/Vis spectroscopy (Fig. S10) showed that the PBI-A is still adsorbed and still in its highly-aggregated state after the experiment (Huang-Rhys factor unchanged). Type B films also decomposed over several hundred cycles. We attribute the loss in conductivity after hundreds of cycles to the decomposition of the underlying FTO, as the portions of FTO not coated in TiO_2/PBI had turned brown post-reaction, consistent with Sn reduction in the FTO. This has been observed by us and others previously,[15, 35] and the operational lifetime of FTO/TiO_2 electrodes has been extended by applying a thin (10 nm) layer of TiO_2 to the FTO by atomic layer deposition (ALD) to prevent corrosion.[15] This ALD approach has found increasing use with unstable or metastable oxides for various photoelectrochemical applications in recent years.[36] The decomposition of the underlying substrate is therefore the limiting factor in device efficiency and longevity using FTO/TiO_2/PBI-A films for electrochromism, which has been observed previously using electrochromic WO_3 on FTO substrates.[37]

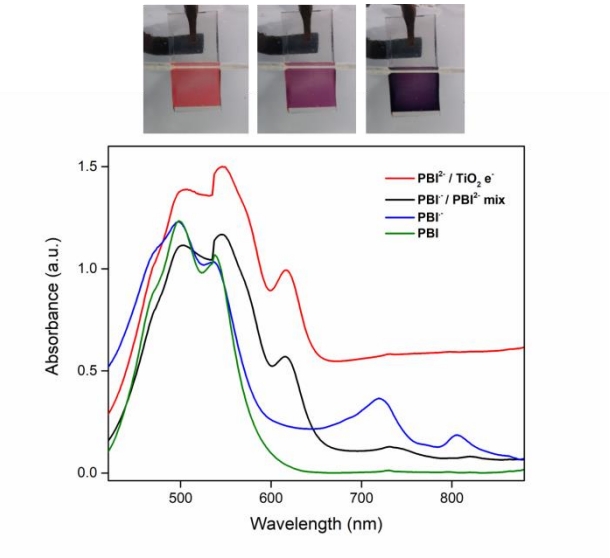

Fig. 4, top: Electrochromic response of a type A H_2O/TiO_2 film as a function of applied potential showing red (fully oxidized PBI-A at open circuit potential), purple (reduced PBI-A, -1.0 V) and navy (reduced TiO_2, -1.5 V) forms. Electrode was ca. 1.2 cm in diameter. **Below:** UV/Vis spectra showing the sequential formation of the one and two-electron reduced PBIs, followed by TiO_2 reduction.

These encouraging results show that the PBI-A/TiO_2 appears to be very stable to cycling on the order of 500x times, that the PBI-A does not show any notable quantity of decomposition or desorption, and that device performance is limited by the underlying substrate and not the PBI. These findings suggest that PBI/TiO_2 composites are highly promising for future use in electrochromics.

Conclusions

TiO_2 nanoparticle electrodes have been used for successful immobilisation of alanine-appended PBI via chemisorption of the carboxylic acid group of the amino acid. By changing the soaking solvent, the degree of PBI-A aggregation in solution could be reduced from highly aggregated in H_2O to monomer-like in MeOH, at equimolar concentrations. This degree of aggregation is transferred onto the TiO_2 surface with soaking, as observed by UV/Vis spectroscopy and FESEM of the soaked films. Cyclic voltammetry of the films revealed the presence of two reversible PBI-based redox processes, known to be the PBI/$PBI^{\cdot-}$ and $PBI^{\cdot-}/PBI^{2-}$ redox couples, which are closely overlapping. Scan rate dependent voltammetry revealed a linear relationship between scan rate and peak current, indicating that a surface-confined electrochemical response dominates, and surface coverages on the order of 10^{-9} $mol.cm^{-2}$ were measured. The response of the film to redox cycling was highly dependent on the solvent and electrolyte composition, and films soaked from H_2O showed distorted voltammetry consistent with a resistive film, while FESEM revealed that the aggregated PBI structures partially blocks the mesopores of the TiO_2, restricting electrolyte diffusion. The electrochromic response of the films was recorded as function of applied potential at 715 nm, the λ_{max} of $PBI^{\cdot-}$. A reversible response was recorded and after 500 cycles the structure of adsorbed PBI-A on the surface was shown by UV/Vis spectroscopy to be largely unchanged. The fact that the PBI-A avoids degradation has implications for the use of such organic materials in electrochromic devices, as organics can be unstable under conditions of extended cycling,[38, 39] and these highly promising results suggest that inorganic-organic hybrid materials based on PBI have great potential as electrochromic devices. After 500 cycles the film becomes increasingly resistive and the FTO background is observed to turn brown, consistent with decomposition of the underlying substrate. FTO decomposition is known to be an issue at reductive

potentials and is attributed to the irreversible reduction of Sn in the FTO.[35] In future work, atomic layer deposition will be used to protect the surface of the FTO from corrosion and extend the lifetime of the device. Additionally, bay-substituted PBI-A will be synthesised to reduce potential aggregation to a minimum,[19] which will optimise device kinetics by ensuring fast interfacial electron transfer and facile electrolyte diffusion. The use of such PBI/TiO_2 films in DSSCs will also be investigated.

Conflicts of interest

There are no conflicts to declare.

Acknowledgements

This publication has emanated from research conducted with the financial support of Science Foundation Ireland (SFI) under the Grant No. 15/SIRG/3517 (JJW). ERD thanks the Leverhulme Trust for an Early Career Fellowship (ECF-2017-223) and the University of Glasgow for a LKAS Fellowship. JJW thanks Prof. Robert J. Forster (DCU) for his ongoing support for the SIRG programme. Thanks to Dr. Darragh Byrne and Prof. Enda McGlynn (DCU) for providing access to the tube furnace for TiO_2 annealing.

Notes and references

1 F. Würthner, C. R. Saha-Möller, B. Fimmel, S. Ogi, P. Leowanawat and D. Schmidt, Chem. Rev., 2016, 116, 962–1052.

2 D. Adams, M. Nolan, J. J. Walsh, L. Mears, A. J. Cowan, E. Draper, B. Dietrich, M. Wallace, M. Barrow and S. M. King, J. Mater. Chem. A, 2017, 5, 7555–7563.

3 S. Chen, P. Slattum, C. Wang and L. Zang, Chem. Rev., 2015, 115, 11967–11998.

4 T. Ye, R. Singh, H.-J. Butt, G. Floudas and P. E. Keivanidis, ACS Appl. Mater. Interfaces, 2013, 5, 11844–57.

5 B. P. Jiang, D. S. Guo and Y. Liu, J. Org. Chem., 2010, 75, 7258–7264.

6 J. Sol, V. Dehm, R. Hecht, F. Würthner, A. Schenning and M. Debije, Angew. Chemie Int. Ed., 2017, 1030–1033.

7 E. R. Draper, J. J. Walsh, T. O. McDonald, M. A. Zwijnenburg, P. J. Cameron, A. J. Cowan and D. J. Adams, J. Mater. Chem. C, 2014, 2, 5570–5575.

8 J. J. Walsh, J. R. Lee, E. R. Draper, S. M. King, F. Jäckel, M. A. Zwijnenburg, D. J. Adams and A. J. Cowan, J. Phys. Chem. C, 2016, 120, 18479–18486.

9 S. Yagai, M. Usui, T. Seki, H. Murayama, Y. Kikkawa, S. Uemura, T. Karatsu, A. Kitamura, A. Asano and S. Seki, J. Am. Chem. Soc., 2012, 134, 7983–94.

10 Y. Shibano, T. Umeyama, Y. Matano and H. Imahori, Org. Lett., 2007, 9, 1971–1974.

11 M. K. Brennaman, M. R. Norris, M. K. Gish, E. M. Grumstrup, L. Alibabaei, D. L. Ashford, A. M. Lapides, J. M. Papanikolas, J. L. Templeton and T. J. Meyer, J. Phys. Chem. Lett., 2015, 6, 4736–4742.

12 E. A. Margulies, L. E. Shoer, S. W. Eaton and M. R. Wasielewski, Phys. Chem. Chem. Phys., 2014, 16, 23735–23742.

13 M. Grätzel, J. Photochem. Photobiol. C Photochem. Rev., 2003, 4, 145–153.

14 T. E. Rosser, C. D. Windle and E. Reisner, Angew. Chemie - Int. Ed., 2016, 55, 7388–7392.

15 J. J. Walsh, M. Forster, C. Smith, G. Neri, R. Potter and A. J. Cowan, Phys. Chem. Chem. Phys., 2018, 20, 6811–6816.

16 S. Usai and J. J. Walsh, J. Electroanal. Chem., 2018, 815, 86–89.

17 J. T. Kirner, J. J. Stracke, B. A. Gregg and R. G. Finke, ACS Appl. Mater. Interfaces, 2014, 6, 13367–13377.

18 F. Ronconi, Z. Syrgiannis, A. Bonasera, M. Prato, R. Argazzi, S. Caramori, V. Cristino and C. A. Bignozzi, J. Am. Chem. Soc., 2015, 137, 150402144705002.

19 B. Shan, A. Nayak, M. K. Brennaman, M. Liu, S. L. Marquard, M. S. Eberhart, T. J. Meyer, B. Shan, A. Nayak, M. K. Brennaman, M. Liu, S. L. Marquard, S. Michael and T. J. Meyer, J. Am. Chem. Soc., 2018, 140, 6493–6500.

20 W. Ma, L. Qin, Y. Gao, W. Zhang, Z. Xie, B. Yang, L. Liu and Y. Ma, Chem. Commun., 2016, 52, 13600–13603.

21 D. Görl, X. Zhang and F. Würthner, Angew. Chemie - Int. Ed., 2012, 51, 6328–6348.

22 S. Ardo, D. Achey, A. J. Morris, M. Abrahamsson and G. J. Meyer, J. Am. Chem. Soc., 2011, 133, 16572–16580.

23 G. Boschloo and D. Fitzmaurice, J. Phys. Chem. B, 1999, 103, 7860–7868.

24 W. J. Hee, M. A. Alghoul, B. Bakhtyar, O. Elayeb, M. A. Shameri, M. S. Alrubaih and K. Sopian, Renew. Sustain. Energy Rev., 2015, 42, 323–343.

25 R. Baetens, B. P. Jelle and A. Gustavsen, Sol. Energy Mater. Sol. Cells, 2010, 94, 87–105.

26 Y. Ke, C. Zhou, Y. Zhou, S. Wang, S. H. Chan and Y. Long, Adv. Funct. Mater., 2018, 1800113, 1800113.

27 C. G. Granqvist, Sol. Energy Mater. Sol. Cells, 2000, 60, 201–262.

28 W. T. Neo, Q. Ye, S.-J. Chua and J. Xu, J. Mater. Chem. C, 2016, 4, 7364–7376.

29 J. A. Kerszulis, K. E. Johnson, M. Kuepfert, D. Khoshabo, A. L. Dyer and J. R. Reynolds, J. Mater. Chem. C, 2015, 3, 3211–3218.

30 A. L. Dyer, E. J. Thompson and J. R. Reynolds, ACS Appl. Mater. Interfaces, 2011, 3, 1787–1795.

31 J. Palenzuela, A. Viñuales, I. Odriozola, G. Cabañero, H. J. Grande and V. Ruiz, ACS Appl. Mater. Interfaces, 2014, 6, 14562–14567.

32 Q. Zeng, A. McNally, T. E. Keyes and R. J. Forster, Electrochem. commun., 2008, 10, 466–470.

33 N. V. Talagaeva, E. V. Zolotukhina, P. A. Pisareva and M. A. Vorotyntsev, J. Solid State Electrochem., 2016, 20, 1235–1240.

34 J. H. Kang, Y. J. Oh, S. M. Paek, S. J. Hwang and J. H. Choy, Sol. Energy Mater. Sol. Cells, 2009, 93, 2040–2044.

35 J. D. Benck, B. A. Pinaud, Y. Gorlin and T. F. Jaramillo, PLoS One, , DOI:10.1371/journal.pone.0107942.

36 S. Hu, N. S. Lewis, J. W. Ager, J. Yang, J. R. McKone and N. C. Strandwitz, J. Phys. Chem. C, 2015, 119, 24201–24228.

37 S. Darmawi, S. Burkhardt, T. Leichtweiss, D. A. Weber, S. Wenzel, J. Janek, M. T. Elm and P. J. Klar, Phys. Chem. Chem. Phys., 2015, 17, 15903–15911.

38 S. W. Huang and K. C. Ho, Sol. Energy Mater. Sol. Cells, 2006, 90, 491–505.

39 N. Kobayashi, S. Miura, M. Nishimura and H. Urano, Sol. Energy Mater. Sol. Cells, 2008, 92, 136–139.